

Polarization-entangled photon pair source using beam displacers and thin crystals

MINJAE HONG,^{1,2,3,4} RODRIGO GÓMEZ,^{1,2} VALERIO FLAVIO GILI,¹
JORGE FUENZALIDA,⁵ AND MARKUS GRÄFE^{1,5,*}

¹*Fraunhofer Institute for Applied Optics and Precision Engineering IOF, Albert-Einstein-Str. 7, 07745 Jena, Germany*

²*Friedrich Schiller University Jena, Abbe Center of Photonics, Albert-Einstein-Str. 6, 07745 Jena, Germany*

³*Technical University of Darmstadt, Department of Physics, Institute for Applied Physics, Schloßgartenstraße 7, 64289 Darmstadt, Germany*

³ *Present address: Max Planck Institute for the Science of Light, Staudtstraße 2, 91058 Erlangen, Germany*

⁴ *Present address: Friedrich Alexander University, Schloßplatz 4, 91058 Erlangen, Germany*

⁵*Technical University of Darmstadt, Department of Physics, Institute for Applied Physics, Schloßgartenstraße 7, 64289 Darmstadt, Germany*

*markus.graefe@tu-darmstadt.de

Abstract: We present an experimental implementation of a polarization-entangled photon pair source based on beam displacers. The down-converted photons are emitted via spontaneous parametric down-conversion in a non-degenerate and type-0 process. We obtain a state fidelity of $F = 0.975 \pm 0.004$ and violate a Clauser-Horne-Shimony-Holt inequality with $S = 2.75 \pm 0.01$. Our source also uses thin crystals for applications in quantum imaging, taking advantage of the large number of spatial modes. With this configuration, we obtain 550 ± 12 spatial modes.

The generation of entangled photon pairs is of paramount importance for quantum technologies such as quantum imaging and sensing [1, 2] and quantum cryptography [3]. Spontaneous parametric down-conversion (SPDC) is the most well-known process for this task wherein a pump photon is down-converted to two photons, namely, signal and idler [4, 5]. Down-converted photons offer entanglement in various degrees of freedom [6] or entanglement can be prepared in a specific degree of freedom through the use of interferometers [7, 8]. By entangling more than one degree of freedom, the so-called hyper-entangled states are obtained. These states have several applications in different areas of quantum physics, ranging from distillation [9], and frequency [10] and spatial multiplexing [11, 12] in quantum communications to holography [13] and super-sensitivity [14] in quantum imaging. Thus, these states deliver several advantages that, in most cases, cannot be achieved with only two qubits-entangled states.

To generate polarization-entanglement using interferometers, one might require dual-wavelength optical components, active stabilization, and demanding alignment. An alternative configuration that relaxes these requirements was introduced by M. Fiorentino and R. G. Beausoleil [15] by employing beam displacers (BD). These devices are polarization-dependent birefringent materials that produce an angular deviation on an impinging optical field, see Fig. 1. Therefore, after the beam has traversed a BD, it can be spatially separated into two transverse locations, where the distance separation depends on the field polarization, its wavelength, and the BD's crystal length and material. Polarization-entanglement sources using beam displacers have been experimentally tested for degenerated [16, 17] and non-degenerated SPDC [18, 19] and for non-degenerated four-wave mixing [20]. Our approach utilizes double displacements [18] of non-degenerated photons and uses two thin crystals for SPDC. The thin crystals produce high-spatial correlations between signal-idler photons, thus being ideal but not limited to quantum imaging applications.

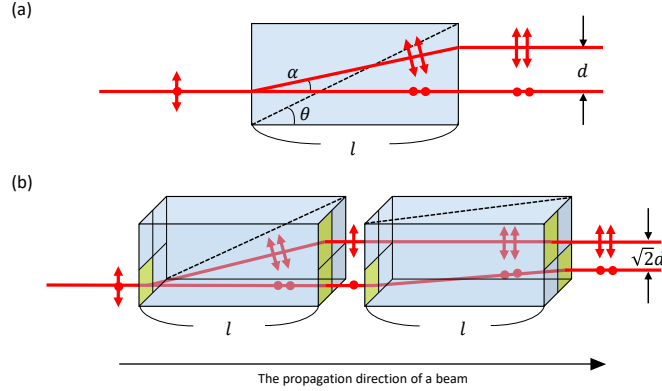


Fig. 1. Beam displacer action in longitudinal-transverse axes. Dashed lines are the direction of an optical axis.

In terms of polarization the desired state shall be a Bell state [21, 22] of the form

$$|\Phi^-\rangle = \frac{1}{\sqrt{2}} (|H_s\rangle |H_i\rangle - |V_s\rangle |V_i\rangle). \quad (1)$$

Here, s (i) stands for signal (idler) photon, and H and V are horizontal and vertical polarizations, respectively. Our experimental setup is depicted in Fig. 2. For generating the state in Eq. (1), we start with a CW 405 nm pump laser that traverses a combination of plate retarders in order to change its polarization and the relative phase between H and V . We initially prepare the pump beam in the diagonal polarization (D). Later, a lens focused the pump beam at the source's plane. Before reaching the nonlinear crystals, the two components of the pump beam, H and V , are spatially separated by two consecutive BDs. The BD has two optical axes: the ordinary axis (polarization independent with refractive index — n_o) and the extra-ordinary axis (polarization dependent with refractive index— n_e). Thus, the impinging optical field is split into two rays inside the BD, forming an angle α ; see Fig. 1(a). This angular deviation depends on the polarization and the BD's angle θ by

$$\tan(\alpha) = \left(\frac{1 - n_o^2}{n_e^2} \right) \frac{\tan(\theta)}{(1 + n_o^2/n_e^2) \tan^2(\theta)}, \quad (2)$$

where $(n_e^2(\theta))^{-1} = \cos^2(\theta)/n_o^2 + \sin^2(\theta)/n_e^2$. In our experiment, the axes of the two consecutive BDs are rotated by 90 degrees [18]. By this, the two polarizations (H and V) are displaced into two orthogonal directions (e.g., 'up' and 'left') in the transverse plane, and in this way, no extra phase needs to be compensated; see Fig. 1(b). In our experiment, we aim for a beam separation of $d = 0.5$ mm, thus obtaining a total separation of ~ 0.71 mm after crossing the two BDs. The beam displacers' lengths can be calculated with the Sellmeier equation that relates the refractive indices and wavelengths of the fields involved by

$$n^2(\lambda) = K + \frac{Q_1 \lambda^2}{\lambda^2 - P_1} + \frac{Q_2 \lambda^2}{\lambda^2 - P_2}. \quad (3)$$

For alpha-barium borate, the parameters in Eq. (3) correspond to $K = 2.67579$, $Q_1 = 0.02009$, $Q_2 = 0.00528$, $P_1 = 0.00470$, and $P_2 = 0$, which are quoted for the wavelength in micrometers. Using Eqs. (2) and (3), and $\lambda_p = 405$ nm, we obtained the crystal length $l_p = 12.52$ mm for the

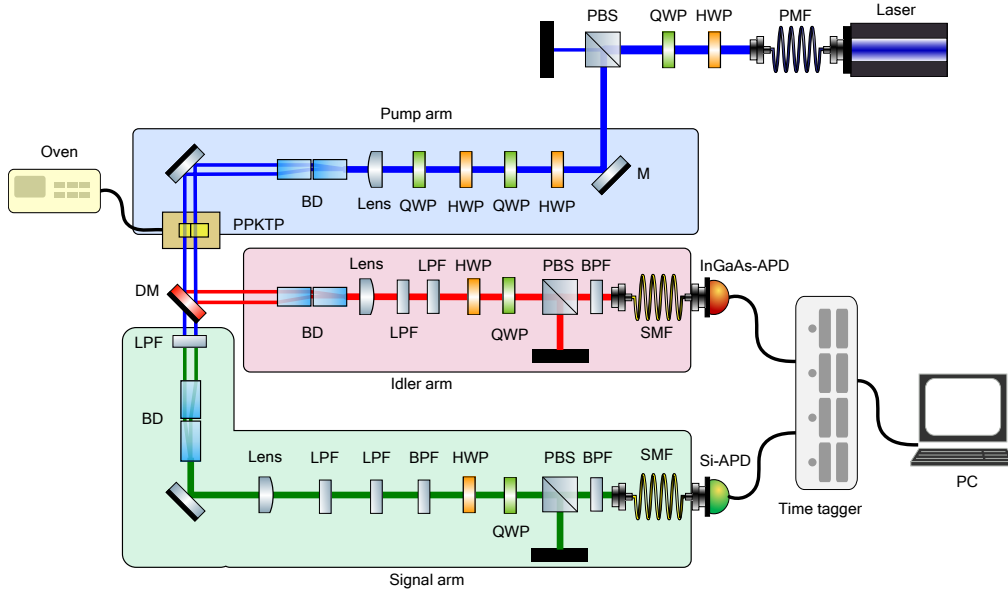


Fig. 2. Setup. A CW 405 nm pump laser is splitted by a pair of beam displacers into two spatial paths. These two pump beams carry an orthogonal polarization with respect to each other. Then, the pumps impinging one nonlinear crystal each, creating a photon pair in a non-degenerate, type-0 SPDC process. The idler and signal photon have wavelengths $\lambda_s = 548.2$ nm and $\lambda_i = 1550$ nm, respectively. Down-converted photons are split with the help of a dichroic mirror; the signal is transmitted, and the idler is reflected. On idler and signal paths, two BDs recombine their optical paths and, therefore, erase their path information. In this way, signal-idler photons are in the state shown in Eq. (1). The signal photon traverses a polarization analysis module composed of a QWP, a HWP, and PBS and later is collected by an SMF. Same for the idler photon. Coincidences of signal-idler photons are counted with a time-tagging module. More details in the main text.

pump beam.

After the action of the first two BDs, the pump beam has been split into two spatially separated positions, where each of which carries an orthogonal polarization with respect to the other. These pump beams illuminate two nonlinear crystals to produce photon pairs through a type-0, non-degenerated SPDC process. The pump ($\lambda_p = 405$ nm) photon is down-converted to a signal ($\lambda_s = 548.2$ nm) and an idler ($\lambda_i = 1550$ nm) photons. Both sources are identical; periodically poled potassium titanyl phosphate (PPKTP) crystal with dimensions of $1 \times 2 \times 2$ mm³ and a poling period of 4.225 μ m. The crystals are in a cross-crystal configuration (in the transverse plane) such that one of them produces the states $|H_s\rangle |H_i\rangle$ while the other generates $|V_s\rangle |V_i\rangle$. Signal and idler photons are split with the help of a dichroic mirror. The reflected idler beams are recombined with two identical BDs of length $l_i = 13.66$ mm. Similarly, the transmitted signal beams are recombined with two identical BDs of length $l_s = 12.98$ mm. In this way, the path information of the signal-idler pair is erased, and the Bell state in Eq. (1) is generated.

In the polarization analysis modules, there is a cascade of a half-wave plate ($HWP_{s/i}$), a quarter-wave plate ($QWP_{s/i}$), and a polarizing beam splitter ($PBS_{s/i}$) in signal and idler arms. Since QWPs are employed only for tomography reconstruction, we will assume they are set at

their fast axis until then. Each PBS is oriented in such a way that it transmits horizontal and reflects vertical polarizations. Signal (idler) photon is spectrally cleaned with an interference filter with a band-pass of 548 ± 6 nm (1550 ± 3 nm) before being collected by a single-mode fiber placed at the horizontal output of its PBS. Signal photons are detected with a single-photon avalanche diode device with a detection efficiency of 55%. For idler photons, an indium gallium arsenide (InGaAs) device with a detection efficiency of 25% is used. Coincidence count rates ($C(s, i) \propto \langle \Phi^+ | E_i^- E_s^- E_i^+ E_s^+ | \Phi^+ \rangle$, E: electric field operator) of signal-idler pairs are counted with a time-tagging module.

To verify polarization entanglement of the bi-photon state, we performed different measurements that are prepared by changing the angle of the retarders HWP_s and HWP_i and checking for the coincidences. The first measurement corresponds to the visibility (\mathcal{V}) between the signal-idler pair in the H/V and D/A bases, where A stands for anti-diagonal polarization. On H/V basis, we have

$$\mathcal{V}_{H/V} = \frac{C(H, H) + C(V, V) - C(H, V) - C(V, H)}{C(H, H) + C(V, V) + C(H, V) + C(V, H)}, \quad (4)$$

where $C(m, n)$ corresponds to a signal-idler coincidence detection in the transmitted outputs of the PBSs at HWPs' angles m and n in signal and idler paths, respectively. These coincidence values are obtained by placing the retarders HWP_s and HWP_i at angles ($H = 0^\circ$, $V = 45^\circ$). The visibility in the D/A basis is similarly computed; however, the angles of HWP_s and HWP_i are changed to ($D = 22.5^\circ$, $A = -22.5^\circ$). In H/V basis we obtained a visibility of $\mathcal{V}_{H/V} = 98.4 \pm 0.1$ whereas in D/A basis $\mathcal{V}_{D/A} = 94.7 \pm 0.2$. Figure 3 depicts the experimental coincidences plot for a fixed HWP_i angle while HWP_s is varied.

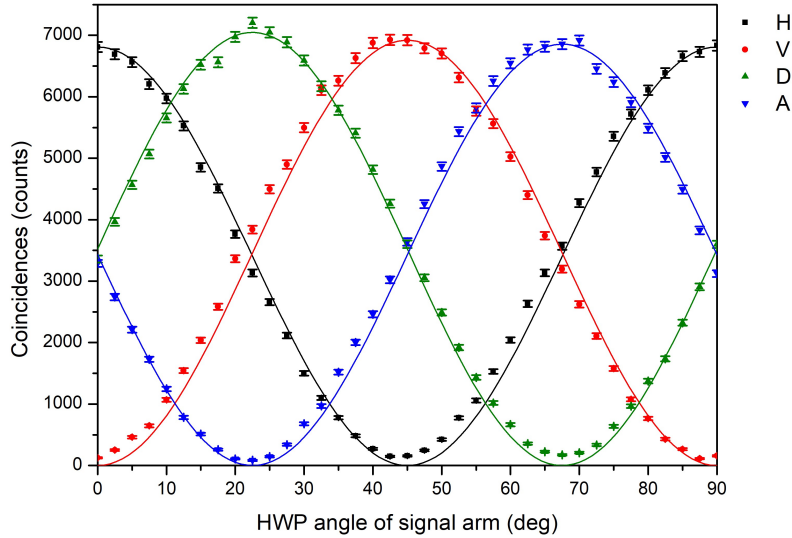


Fig. 3. Coincidence detection in each basis. Dots are experimental data and lines are theoretical fitting. Colors differ by the polarization of idler photon polarization: black - horizontal polarization, red - vertical polarization, green - diagonal polarization, blue - anti-diagonal polarization.

In a second experiment, we test the Clauser-Horne-Shimony-Holt (CHSH) inequality [23], which is a standard technique to quantify entanglement in a bipartite quantum system. The CHSH inequality can be expressed as

$$\mathcal{S} = \mathcal{E}(m_1, n_1) + \mathcal{E}(m_2, n_2) + \mathcal{E}(m_1, n_2) - \mathcal{E}(m_2, n_1), \quad (5)$$

where

$$\mathcal{E}(m, n) = \frac{C(m, n) + C(m^\perp, n^\perp) - C(m^\perp, n) - C(m, n^\perp)}{C(m, n) + C(m^\perp, n^\perp) + C(m^\perp, n) + C(m, n^\perp)}. \quad (6)$$

$C(m, n)$ still corresponds to a joint detection between the transmitted outputs of the PBSs at HWPs' angles m and n , while m^\perp and n^\perp denote the reflected outputs of the PBSs for the same angles. Since we used only the transmitted output of the PBSs, the angles employed in our setup for the CHSH inequality are ($m_1 = 0^\circ, m_1^\perp = 45^\circ, m_2 = 22.5^\circ, m_2^\perp = 67.5^\circ$) for HWP_s, and ($n_1 = 11.25^\circ, n_1^\perp = 33.75^\circ, n_2 = 56.25^\circ, n_2^\perp = 78.25^\circ$) for HWP_i. By doing this, we obtained a value for the CHSH inequality of $\mathcal{S} = 2.75 \pm 0.01$, demonstrating a high violation from the classical limit of $\mathcal{S} = 2$ by 75 standard deviations.

In a last experiment regarding polarization entanglement, we perform a quantum state tomography [24] of the Bell state in Eq. (1). To reconstruct the density matrix, and following previous notation, we measure signal-idler coincidences using the following combinations $C(H, H), C(H, D), C(H, V), C(H, L), C(V, H), C(V, D), C(V, V), C(V, L), C(D, H), C(D, D), C(D, V), C(D, R), C(R, H), C(R, D), C(R, V)$, and $C(R, L)$. R (L) stands for right (left) circular polarized light and can be prepared by rotating a QWP at 45° (-45°). In this way, the reconstructed density matrix $\hat{\rho}_{\text{exp}}$ is

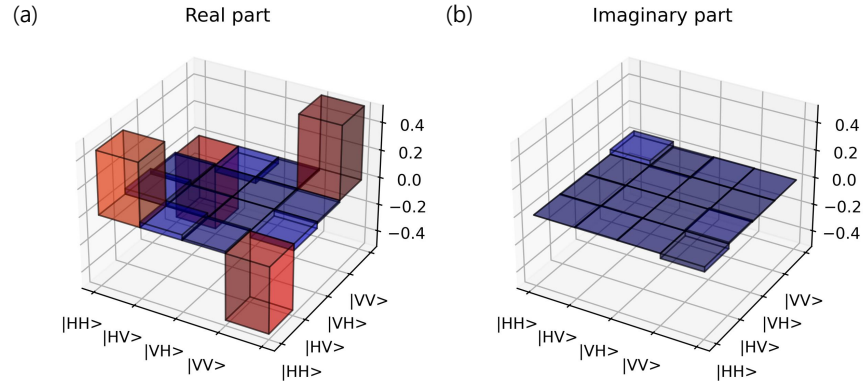


Fig. 4. Density matrix reconstruction. (a) Real part and (b) imaginary part.

$$\hat{\rho}_{\text{exp}} = \begin{pmatrix} 0.4580 & 0.0386 + i0.0050 & 0.0142 + i0.0014 & -0.4802 + i0.0348 \\ 0.039 - i0.0050 & 0.0078 & 0.0002 - i0.0005 & -0.048 + i0.0107 \\ 0.0014 - i0.0014 & 0.0002 + i0.0005 & 0.0007 & -0.0144 - i0.0022 \\ -0.4802 - i0.0348 & 0.0481 - i0.01069 & -0.01445 + i0.0022 & 0.5335 \end{pmatrix}. \quad (7)$$

The fidelity of our state, $F(\hat{\rho}_{\text{exp}}, \hat{\rho}_{\text{th}}) = \left\{ \text{tr} \left(\sqrt{\sqrt{\hat{\rho}_{\text{exp}}} \hat{\rho}_{\text{th}} \sqrt{\hat{\rho}_{\text{exp}}}} \right) \right\}^2$, where $\hat{\rho}_{\text{th}} = |\Phi^-\rangle \langle \Phi^-|$ is the density matrix of Eq. (1), is $F = 0.975 \pm 0.004$. The error was obtained by the Gaussian estimation. Figures 4(a) and 4(b) show the real part and the imaginary part of $\hat{\rho}_{\text{exp}}$, respectively.

In quantum imaging, there are plenty of techniques to estimate bi-photon spatial correlations [25–30]. Here, we decide to include a parameter that is ultimately associated with the source's properties. The number of spatial modes produced by a crystal of length l_c and refractive index n_s (n_i) for signal (idler) photon is given by [31,32]

$$N_{\text{modes}} = \frac{5.56 \pi w_p^2 n_i n_s}{\ln(2) l_c (\lambda_i n_s + \lambda_s n_i)} \quad (8)$$

w_p stands for the pump waist. Evidently, N in Eq. (8), can be enhanced by decreasing the length of the nonlinear crystals. We perform an estimation of the spatial modes produced by our specific source. For this, we measured w_p with a transverse translation stage and a power meter.

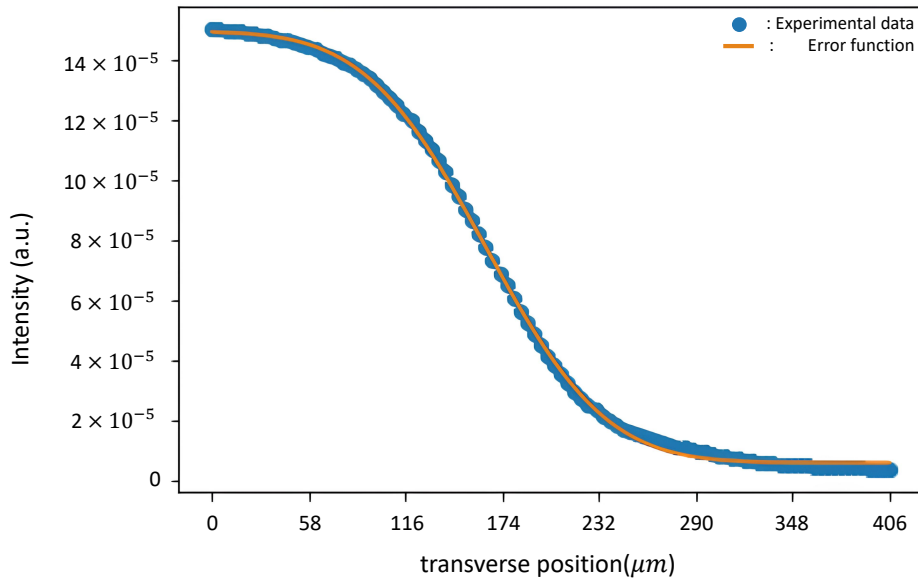


Fig. 5. Measurement of the beam waist by a translation stage and a power meter. Intensity was measured at each transverse position (blue dots). The beam waist was estimated by fitting an Error function (orange line).

Figure 5 shows the experimental results for the beam waist measurement. We obtained a beam waist of $229 \pm 2.5 \mu\text{m}$ from an Error function fitting, and thus, the number of spatial modes estimated by Eq. (8) was 550 ± 12 . It is noteworthy that our source implies a large number of modes. Sharper spatial correlations increase with the number of spatial modes, meaning that

our source, which carries polarization-space hyper-entanglement, has promising applications in quantum imaging. A larger number of spatial modes can be achievable by increasing the pump waist size, which is ultimately limited by the crystal aperture of $1 \times 2 \text{ mm}^2$ in our case.

We have experimentally introduced a new polarization-entangled photon pair source using beam displacers for quantum imaging applications. The novelty of our experiment resides in the wavelengths employed ($\lambda_s = 548.2 \text{ nm}$ and $\lambda_i = 1550 \text{ nm}$), the tunable spatial indistinguishability for wide-field imaging, and the optimization employing thin nonlinear crystals. In our source, the spatial correlations (as well as the number of spatial modes) can be improved by (1) increasing the aperture or (2) reducing the crystal length. For the former, beta barium borate crystals with large apertures are already available on the market. Additionally, for higher photon pair generation, PPKTP crystals with apertures of up to $4 \times 4 \text{ mm}^2$ have recently been introduced [33]. For the latter, nonlinear metasurfaces can be built in lengths in the order of microns [34, 35], which might be an option for reaching the diffraction limit [36, 37] in techniques such as ghost imaging [38, 39] and quantum imaging with undetected photons [40]. Of particular importance, our source can be useful for imaging objects with birefringent properties [41] or quantum imaging distillation [42, 43]. In other areas, such as quantum communication, it has been proven that that distillation can be enhanced by exploiting hyper-entangled states. Hence, our developed source can offer more resilience to noise than techniques only using spatial correlations.

Funding. This research was carried out within the scope of the ICON-Programme of the Fraunhofer Society „Integrated Photonic Solutions for Quantum Technologies (InteQuant)”. We also acknowledge support from the European Union’s Horizon 2020 Research and Innovation Action under Grant Agreement No. 101113901 (Qu-Test, HORIZON-CL4-2022-QUANTUM-05-SGA).

Disclosures. The authors declare no conflicts of interest.

Data Availability Statement. Data underlying the results presented in this paper are not publicly available at this time but may be obtained from the authors upon reasonable request.

References

1. M. Gilaberte Basset, F. Setzpfandt, F. Steinlechner, *et al.*, “Perspectives for applications of quantum imaging,” *Laser Photonics Rev.* **13**, 1900097 (2019).
2. J. Fuenzalida, E. Giese, and M. Gräfe, “Nonlinear interferometry: A new approach for imaging and sensing,” *Adv. Quantum Technol.* p. in press (2024).
3. S. Pirandola, U. L. Andersen, L. Banchi, *et al.*, “Advances in quantum cryptography,” *Adv. Opt. Photon.* **12**, 1012–1236 (2020).
4. D. Klyshko, “Scattering of light in a medium with nonlinear polarizability,” *Sov. Phys. JETP* **28**, 522 (1969).
5. D. C. Burnham and D. L. Weinberg, “Observation of simultaneity in parametric production of optical photon pairs,” *Phys. Rev. Lett.* **25**, 84 (1970).
6. S. P. Walborn, C. Monken, S. Pádua, and P. S. Ribeiro, “Spatial correlations in parametric down-conversion,” *Phys. Rep.* **495**, 87–139 (2010).
7. A. Anwar, C. Perumangatt, F. Steinlechner, *et al.*, “Entangled photon-pair sources based on three-wave mixing in bulk crystals,” *Rev. Sci. Instruments* **92**, 041101 (2021).
8. M. Erhard, M. Krenn, and A. Zeilinger, “Advances in high-dimensional quantum entanglement,” *Nat. Rev. Phys.* **2**, 365–381 (2020).
9. S. Ecker, P. Sohr, L. Bulla, *et al.*, “Experimental single-copy entanglement distillation,” *Phys. Rev. Lett.* **127**, 040506 (2021).
10. E. Brambila, R. Gómez, R. Fazili, *et al.*, “Ultrabright polarization-entangled photon pair source for frequency-multiplexed quantum communication in free-space,” *Opt. Express* **31**, 16107–16117 (2023).
11. E. A. Ortega, K. Dovzhik, J. Fuenzalida, *et al.*, “Experimental space-division multiplexed polarization-entanglement distribution through 12 paths of a multicore fiber,” *PRX Quantum* **2**, 040356 (2021).
12. E. A. Ortega, J. Fuenzalida, K. Dovzhik, *et al.*, “Implementation of space-division multiplexed entanglement-based quantum cryptography over multicore fiber,” *arXiv preprint arXiv:2401.04327* (2024).
13. H. Defienne, B. Ndagano, A. Lyons, and D. Faccio, “Polarization entanglement-enabled quantum holography,” *Nat. Phys.* **17**, 591–597 (2021).
14. R. Camphausen, Á. Cuevas, L. Duempelmann, *et al.*, “A quantum-enhanced wide-field phase imager,” *Sci. Adv.* **7**, eabj2155 (2021).

15. M. Fiorentino and R. G. Beausoleil, "Compact sources of polarization-entangled photons," *Opt. Express* **16**, 20149–20156 (2008).
16. P. G. Evans, R. S. Bennink, W. P. Grice, et al., "Bright source of spectrally uncorrelated polarization-entangled photons with nearly single-mode emission," *Phys. Rev. Lett.* **105**, 253601 (2010).
17. A. Lohrmann, C. Perumangatt, A. Villar, and A. Ling, "Broadband pumped polarization entangled photon-pair source in a linear beam displacement interferometer," *Appl. Phys. Lett.* **116**, 021101 (2020).
18. R. Horn and T. Jennewein, "Auto-balancing and robust interferometer designs for polarization entangled photon sources," *Opt. Express* **27**, 17369–17376 (2019).
19. L. Shen, C. H. Chow, J. Y. X. Peh, et al., "Distributing polarization-entangled photon pairs with high rate over long distances through standard telecommunication fiber," *Phys. Rev. Appl.* **18**, 044075 (2022).
20. Y. S. Lee, M. Xie, R. Tannous, and T. Jennewein, "Sagnac-type entangled photon source using only conventional polarization optics," *Quantum Sci. Technol.* **6**, 025004 (2021).
21. A. Einstein, B. Podolsky, and N. Rosen, "Can quantum-mechanical description of physical reality be considered complete?" *Phys. Rev.* **47**, 777–780 (1935).
22. J. S. Bell, "On the einstein podolsky rosen paradox," *Phys. Phys. Fiz.* **1**, 195–200 (1964).
23. J. F. Clauser, M. A. Horne, A. Shimony, and R. A. Holt, "Proposed experiment to test local hidden-variable theories," *Phys. Rev. Lett.* **23**, 880–884 (1969).
24. D. F. V. James, P. G. Kwiat, W. J. Munro, and A. G. White, "Measurement of qubits," *Phys. Rev. A* **64**, 052312 (2001).
25. C. K. Law and J. H. Eberly, "Analysis and interpretation of high transverse entanglement in optical parametric down conversion," *Phys. Rev. Lett.* **92**, 127903 (2004).
26. H. Di Lorenzo Pires, C. H. Monken, and M. P. van Exter, "Direct measurement of transverse-mode entanglement in two-photon states," *Phys. Rev. A* **80**, 022307 (2009).
27. J. C. Howell, R. S. Bennink, S. J. Bentley, and R. W. Boyd, "Realization of the einstein-podolsky-rosen paradox using momentum- and position-entangled photons from spontaneous parametric down conversion," *Phys. Rev. Lett.* **92**, 210403 (2004).
28. L. Achatz, E. A. Ortega, K. Dovzhik, et al., "Certifying position-momentum entanglement at telecommunication wavelengths," *Phys. Scr.* **97**, 015101 (2022).
29. F. Just, A. Cavanna, M. V. Chekhova, and G. Leuchs, "Transverse entanglement of biphotons," *New J. Phys.* **15**, 083015 (2013).
30. M. P. Edgar, D. S. Tasca, F. Izdebski, et al., "Imaging high-dimensional spatial entanglement with a camera," *Nat. Commun.* **3**, 984 (2012).
31. E. Brambilla, A. Gatti, M. Bache, and L. A. Lugiato, "Simultaneous near-field and far-field spatial quantum correlations in the high-gain regime of parametric down-conversion," *Phys. Rev. A* **69**, 023802 (2004).
32. I. Kviatkovsky, H. M. Chrzanowski, E. G. Avery, et al., "Microscopy with undetected photons in the mid-infrared," *Sci. Adv.* **6**, eabd0264 (2020).
33. C. S. Lee, A. Zukauskas, and C. Canalias, "Large-aperture periodically poled rb-doped ktp with a short-period via coercive field engineering," *Opt. Mater. Express* **13**, 2203–2213 (2023).
34. G. Marino, A. S. Solntsev, L. Xu, et al., "Spontaneous photon-pair generation from a dielectric nanoantenna," *Optica* **6**, 1416–1422 (2019).
35. T. Santiago-Cruz, A. Fedotova, V. Sultanov, et al., "Photon pairs from resonant metasurfaces," *Nano letters* **21**, 4423–4429 (2021).
36. V. F. Gili, D. Dupish, A. Vega, et al., "Quantum ghost imaging based on a "looking back" 2d spad array," *Appl. Opt.* **62**, 3093–3099 (2023).
37. A. Vega, E. A. Santos, J. Fuenzalida, et al., "Fundamental resolution limit of quantum imaging with undetected photons," *Phys. Rev. Res.* **4**, 033252 (2022).
38. D. V. Strekalov, A. V. Sergienko, D. N. Klyshko, and Y. H. Shih, "Observation of two-photon "ghost" interference and diffraction," *Phys. Rev. Lett.* **74**, 3600 (1995).
39. T. B. Pittman, Y. H. Shih, D. V. Strekalov, and A. V. Sergienko, "Optical imaging by means of two-photon quantum entanglement," *Phys. Rev. A* **52**, R3429 (1995).
40. G. B. Lemos, V. Borish, G. D. Cole, et al., "Quantum imaging with undetected photons," *Nature* **512**, 409–412 (2014).
41. S. Brasselet and M. A. Alonso, "Polarization microscopy: from ensemble structural imaging to single-molecule 3d orientation and localization microscopy," *Optica* **10**, 1486–1510 (2023).
42. H. Defienne, M. Reichert, J. W. Fleischer, and D. Faccio, "Quantum image distillation," *Sci. Adv.* **5**, eaax0307 (2019).
43. J. Fuenzalida, M. Gilaberte Basset, S. Töpfer, et al., "Experimental quantum imaging distillation with undetected light," *Sci. Adv.* **9**, eadg9573 (2023).